BJR

https://doi.org/10.1259/bjr.20201329

Received: 12 November 2020 | Revised: 03 February 2021 | Accepted: 09 February 2021

Cite this article as:
Noda Y, Kaga T, Kawai N, Miyoshi T, Kawada H, Hyodo F, et al. Low-dose whole-body CT using deep learning image reconstruction: image quality and lesion detection. *Br J Radiol* 2021; **94**: 20201329.

FULL PAPER

Low-dose whole-body CT using deep learning image reconstruction: image quality and lesion detection

[1]YOSHIFUMI NODA, MD, PhD, [1]TETSURO KAGA, MD, [1]NOBUYUKI KAWAI, MD, [1]TOSHIHARU MIYOSHI, [1]HIROSHI KAWADA, MD, [2]FUMINORI HYODO, PhD, [3]AVINASH KAMBADAKONE, MD, FRCR and [1]MASAYUKI MATSUO, MD, PhD

[1]Department of Radiology, Gifu University, 1-1 Yanagido, Gifu 501-1194, Japan
[2]Department of Radiology, Frontier Science for Imaging, Gifu University, 1-1 Yanagido, Gifu 501-1194, Japan
[3]Department of Radiology, Massachusetts General Hospital, Harvard Medical School, Boston, Massachusetts

Address correspondence to: Dr Yoshifumi Noda
E-mail: *noda1031@gifu-u.ac.jp*

Objectives: To evaluate image quality and lesion detection capabilities of low-dose (LD) portal venous phase whole-body computed tomography (CT) using deep learning image reconstruction (DLIR).
Methods: The study cohort of 59 consecutive patients (mean age, 67.2 years) who underwent whole-body LD CT and a prior standard-dose (SD) CT reconstructed with hybrid iterative reconstruction (SD-IR) within one year for surveillance of malignancy were assessed. The LD CT images were reconstructed with hybrid iterative reconstruction of 40% (LD-IR) and DLIR (LD-DLIR). The radiologists independently evaluated image quality (5-point scale) and lesion detection. Attenuation values in Hounsfield units (HU) of the liver, pancreas, spleen, abdominal aorta, and portal vein; the background noise and signal-to-noise ratio (SNR) of the liver, pancreas, and spleen were calculated. Qualitative and quantitative parameters were compared between the SD-IR, LD-IR, and LD-DLIR images. The CT dose-index volumes ($CTDI_{vol}$) and dose-length product (DLP) were compared between SD and LD scans.
Results: The image quality and lesion detection rate of the LD-DLIR was comparable to the SD-IR. The image quality was significantly better in SD-IR than in LD-IR ($p < 0.017$). The attenuation values of all anatomical structures were comparable between the SD-IR and LD-DLIR ($p = 0.28–0.96$). However, background noise was significantly lower in the LD-DLIR ($p < 0.001$) and resulted in improved SNRs ($p < 0.001$) compared to the SD-IR and LD-IR images. The mean $CTDI_{vol}$ and DLP were significantly lower in the LD (2.9 mGy and 216.2 mGy•cm) than in the SD (13.5 mGy and 1011.6 mGy•cm) ($p < 0.0001$).
Conclusion: LD CT images reconstructed with DLIR enable radiation dose reduction of >75% while maintaining image quality and lesion detection rate and superior SNR in comparison to SD-IR.
Advances in knowledge: Deep learning image reconstruction algorithm enables around 80% reduction in radiation dose while maintaining the image quality and lesion detection compared to standard-dose whole-body CT.

INTRODUCTION

Computed tomography (CT) is widely used in benign conditions such as Crohn disease,[1] renal stone[2] or screening of liver in patients with hepatitis[3] as well as in oncological patients for tumor staging, assessment of therapeutic response, tumor recurrence, and presence of new lesions and/or distant metastases.[4,5] Whole-body CT are performed more frequently in patients with low-grade malignancies such as lymphoma or testicular tumors for surveillance. However, repeated CT acquisitions in young patients can lead to increased cumulative radiation dose exposure and expose them to theoretical harmful risks of CT. Radiation dose reduction strategies are paramount in these group of patients. However, reduction in radiation dose often have penalties of increased image noise which can reduce image quality and limit diagnostic performance of the scans.[6]

Iterative reconstruction (IR) techniques (including the hybrid-IR technique and the full-IR technique) enable reduction in image noise. The hybrid-IR technique uses a blend of filtered back-projection (FBP) images with iteratively reconstructed images in the raw data domain to reduce image noise.[7–9] The full-IR does not involve blending with FBP data and could significantly reduce the background noise (10.5–11.2 HU) compared to the 100% hybrid-IR (14.8–15.8 HU).[10] These IR techniques have

enabled radiation dose reduction of 58.2% with hybrid-IR[11] and 74.7% with full-IR,[12] while maintaining or even improving image quality. Multiple different types of IR techniques have been used in several low-dose (LD) CT acquisitions such as CT angiography,[11] contrast-enhanced abdominal CT,[12] and whole-body CT.[13] Despite the benefits of IR techniques, the limitations of this technology include limited ability to detect low-contrast lesions and spatial resolution compared to scans reconstructed with FBP.[14] Additionally, the textural appearance of the CT scans reconstructed with IR algorithms have been variously described as "plasticky".[15]

Recently, the deep learning image reconstruction (DLIR) technique has been proposed to reduce image noise and improve CT image quality.[16,17] The ability to enhance image quality by reducing noise provides opportunities for radiation dose reduction. The DLIR technique also could potentially maintain the ability to detect low contrast lesions without damaging the texture appearance of IR algorithms. However, there are no studies to assess the impact of DLIR on image quality and lesion detection when performed with LD CT techniques. Therefore, this study aimed to evaluate the image quality and lesion detection of LD whole-body CT using DLIR and hybrid-IR, and compare them with standard-dose (SD) whole-body CT using the hybrid-IR technique.

METHODS AND MATERIALS

Patients

Our institutional review board provided ethical approval for this prospective study. Written informed consent was obtained from all patients. In this study, we initially included 78 consecutive patients who underwent contrast-enhanced whole-body CT to screen for tumor metastases and/or recurrence after surgical resection or chemotherapy for malignant tumors between May 2020 and June 2020. Out of these 78 patients, we excluded patients (n = 19) who did not have a prior SD CT within one-year (n = 15) and those with different CT contrast injection protocol (n = 4). The final cohort consisted of 59 patients (25 males and 34 females; mean age ± standard deviation, 67.2 ± 10.2 years; range, 42–89 years). This final cohort included patients with gastric cancer (n = 15), rectal cancer (n = 11), sigmoid colon cancer (n = 7), ascending colon cancer (n = 5), transverse colon cancer (n = 3), renal cancer (n = 3), esophageal cancer (n = 2), uterine cancer (n = 2), descending colon cancer (n = 2), pancreatic cancer (n = 1), malignant sacral bone tumor (n = 1), prostate cancer (n = 1), bile duct cancer (n = 1), breast cancer (n = 1), bladder cancer (n = 1), cecal cancer (n = 1), fallopian tube cancer (n = 1), and ovarian cancer (n = 1). In 89.8% of patients (n = 53/59), the CT was performed as part of post-surgical surveillance after resection of tumor and in 10.2% of patients (n = 6/59), the CT was performed for response assessment following systemic chemotherapy.

CT Technique and Contrast Material Injection

All examinations were performed with a fast kilovoltage-switching dual-energy CT scanner (Revolution CT; GE Healthcare, Milwaukee, WI, USA). All the patients in the study underwent whole-body CT examination consisting of an unenhanced SD scan and a portal venous phase LD whole-body CT, coverage from the submaxillary to the ischium. The CT imaging parameters were as follows: noise index, 14.0 at 5 mm slice collimation; tube current, variable; detector configuration, 128 detectors with 0.625 mm section thickness; rotation time, 0.5 sec; pitch, 0.508:1; scan field-of-view, 50 cm; and display field-of-view, 38 cm. The tube current for LD CT was reduced to attain a CT dose-index volume ($CTDI_{vol}$) and dose-length product (DLP) less than a quarter of the SD CT which was based on prior data. Raw data were reconstructed using an adaptive statistical iteration reconstruction Veo (ASiR-V; GE Healthcare) of 40% (LD-IR image) and high TrueFidelity™ (TFI-H; GE Healthcare) (LD-DLIR image), with 5 mm section thickness and 0% overlap.

All the patients in the cohort had a prior portal venous phase SD whole-body CT examination performed with either Brilliance CT 64 (Philips Medical Systems, Best, the Netherlands [n = 15]), Discovery CT750 HD (GE Healthcare, Milwaukee, WI, USA [n = 29]), or Revolution CT (GE Healthcare [n = 15]). Raw data were reconstructed using hybrid-IR with 5 mm section thickness and

Figure 1. Flow chart of included and excluded patients.

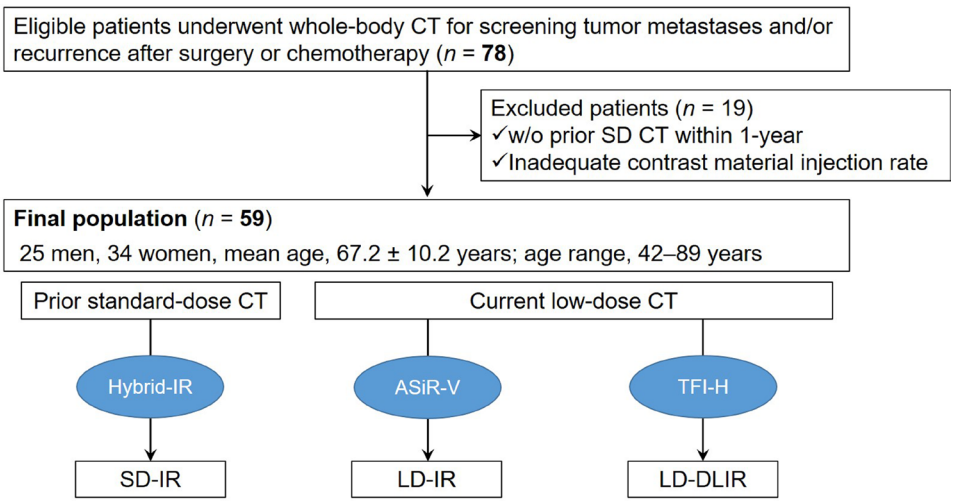

Table 1. CT Scanning Parameters

Parameters	Standard-dose CT			Low-dose CT
CT scanner	Brilliance CT 64	Discovery CT750 HD	Revolution CT	Revolution CT
Tube voltage	120 kVp			
Noise index	N.A.	7	7	14
Tube current	ACS +Z-DOM	Auto mA	Auto mA	Auto mA
Beam collimation	0.625 mm ×64	0.625 mm ×64	0.625 mm ×128	0.625 mm ×128
Rotation time	0.5			
Pitch	0.859:1	0.984:1	0.508:1	0.508:1
Scan field-of-view	50 cm			
Display field-of-view	38 cm			
Kernel	Smooth (A)	STND	STND	STND
Reconstruction	iDose 3	ASiR-V 30%	ASiR-V 40%	ASiR-V 40%/TFI-H

ASiR-V, adaptive statistical iteration reconstruction Veo; NA, not applicable; TFI, TrueFidelity Image.

0% overlap (SD-IR image) (Figure 1). The specific CT imaging parameters are summarized in Table 1.

In all patients, a contrast material (600 mgI/kg body weight) was intravenously injected over a fixed duration of 30 sec. Portal venous phase CT scanning was initiated 70 sec after the injection of the contrast material.[18] The $CTDI_{vol}$ and DLP from the dose report were recorded for current unenhanced SD and portal venous phase LD scans.

Table 2. Patient Demographics and Lesion Characteristics

Patient Demographics	
Age (y)	67.2 ± 10.2 (42–89)
Male:Female	25:34
Body weight (kg)	52.8 ± 10.7 (33.0–82.0)
Body mass index	20.8 ± 3.4 (13.0–29.5)
Lesion Characteristics	**Size (mm)**
Thyroid nodule (n = 32)	7.8 ± 3.4 (3.0–17.7)
Breast mass (n = 2)	8.1 ± 5.1 (4.5–11.7)
Lymphadenopathy (n = 4)	23.1 ± 15.1 (13.5–45.6)
Liver cyst (n = 107)	10.5 ± 10.1 (2.3–59.2)
Hepatic hemangioma (n = 9)	14.8 ± 11.0 (5.3–39.9)
Liver metastasis (n = 18)	20.9 ± 16.5 (5.3–65.4)
Pancreatic cyst (n = 2)	15.2 ± 12.6 (6.3–24.1)
Peritoneal dissemination (n = 5)	14.5 ± 2.0 (12.4–17.0)
Adrenal nodule (n = 2)	14.6 ± 1.8 (13.3–15.8)
Renal cyst (n = 91)	13.5 ± 15.4 (2.4–87.2)
Uterine mass (n = 11)	16.6 ± 10.2 (4.3–36.9)
Ovarian mass (n = 5)	22.4 ± 2.9 (17.9–25.2)

Data are means ± 1 standard deviation with ranges in parentheses.

DEEP LEARNING–BASED IMAGE RECONSTRUCTION

The DLIR technique used for image reconstruction in our study is a vendor specific deep neural network-based recon engine (TrueFidelity™, GE Healthcare). This technology relies on FBP reconstructed CT images as the ground truth for training the reconstruction algorithm using both phantom and clinical cases. The DLIR engine generates output images from input data acquired with LD radiation. The DLIR algorithm allows creation of CT images with low image noise while maintaining the texture, anatomical details, and pathological details similar to FBP reconstructed images. The DLIR engine generates images with a fast reconstruction time for routine clinical use (≤85 s for an abdominal CT scan). Three selectable reconstruction strength levels are available with TFI; low, medium, and high to control the amount of noise reduction.[19] Greffier J et al reported that the radiation dose could be reduced by up to 50% while maintaining lesion detectability, noise texture, and spatial resolution.[20] Because we expected radiation dose in the LD scan to be less than a quarter of the dose in the SD, we applied TFI-H for this study.

QUALITATIVE IMAGE ANALYSIS

Image quality

Two experienced radiologists (T.K. and N.K., with 3 and 8 years of post-training experience in interpreting body CT images, respectively), who were unaware of the reconstruction technique, independently and randomly reviewed whole-body CT images. CT images were initially presented with a preset soft-tissue window setting (350 HU width and 40HU level), and the radiologists were allowed to modify the window setting at their discretion. For each image review, one image series was displayed at a time.

The radiologists evaluated the image quality for sharpness, image noise, and diagnostic acceptability using a 5-point scale: 5 = excellent, 4 = good; 3 = acceptable, 2 = suboptimal, and 1 = unacceptable.

Table 3. Image Quality and Lesion Detection

	SD-IR	LD-IR	LD-DLIR	*p*-value
Image quality				
Sharpness (κ value)	0.31	0.24	0.68	N.A.
Reader 1	4.0 ± 0.2 (4.0–5.0)	3.2 ± 0.4[a] (3.0–4.0)	4.1 ± 0.3 (4.0–5.0)	<0.001
Reader 2	4.1 ± 0.3 (4.0–5.0)	3.4 ± 0.5[a] (3.0–4.0)	4.1 ± 0.3 (4.0–5.0)	<0.001
Image noise (κ value)	0.41	0.66	0.61	N.A.
Reader 1	3.9 ± 0.3 (3.0–4.0)	3.0 ± 0.2[a] (2.0–3.0)	4.1 ± 0.4[b] (3.0–5.0)	<0.001
Reader 2	3.9 ± 0.3 (3.0–5.0)	2.9 ± 0.3[a] (2.0–4.0)	4.2 ± 0.5[b] (3.0–5.0)	<0.001
Diagnostic acceptability (κ value)	0.65	0.59	0.42	N.A.
Reader 1	4.0 ± 0.2 (3.0–4.0)	3.1 ± 0.3[a] (2.0–4.0)	4.1 ± 0.3 (3.0–5.0)	<0.001
Reader 2	4.0 ± 0.3 (3.0–5.0)	3.1 ± 0.4[a] (2.0–4.0)	4.0 ± 0.3 (3.0–5.0)	<0.001
Lesion detection				
Thyroid nodule				
Reader 1	100% (22/22)	100% (22/22)	100% (22/22)	1.00
Reader 2	91% (20/22)	86% (19/22)	86% (19/22)	1.00
Breast mass				
Reader 1	100% (2/2)	100% (2/2)	100% (2/2)	1.00
Reader 2	100% (2/2)	100% (2/2)	100% (2/2)	1.00
Lymphadenopathy				
Reader 1	100% (4/4)	100% (4/4)	100% (4/4)	1.00
Reader 2	100% (4/4)	100% (4/4)	100% (4/4)	1.00
Liver cyst				
Reader 1	100% (34/34)	97% (33/34)	97% (33/34)	1.00
Reader 2	91% (31/34)	91% (31/34)	91% (31/34)	1.00
Hepatic hemangioma				
Reader 1	100% (8/8)	100% (8/8)	100% (8/8)	1.00
Reader 2	88% (7/8)	88% (7/8)	88% (7/8)	1.00
Liver metastasis				
Reader 1	100% (3/3)	100% (3/3)	100% (3/3)	1.00
Reader 2	100% (3/3)	100% (3/3)	100% (3/3)	1.00
Pancreatic cyst				
Reader 1	100% (2/2)	100% (2/2)	100% (2/2)	1.00
Reader 2	100% (2/2)	100% (2/2)	100% (2/2)	1.00
Peritoneal dissemination				
Reader 1	100% (2/2)	100% (2/2)	100% (2/2)	1.00
Reader 2	100% (2/2)	100% (2/2)	100% (2/2)	1.00
Adrenal nodule				
Reader 1	100% (2/2)	100% (2/2)	100% (2/2)	1.00
Reader 2	100% (2/2)	100% (2/2)	100% (2/2)	1.00
Renal cyst				
Reader 1	95% (35/37)	89% (33/37)	95% (35/37)	0.73
Reader 2	100% (37/37)	97% (36/37)	97% (36/37)	1.00

(Continued)

Table 3. (Continued)

	SD-IR	LD-IR	LD-DLIR	*p*-value
Uterine mass				
Reader 1	86% (6/7)	86% (6/7)	86% (6/7)	1.00
Reader 2	86% (6/7)	86% (6/7)	86% (6/7)	1.00
Ovarian mass				
Reader 1	100% (4/4)	100% (4/4)	100% (4/4)	1.00
Reader 2	100% (4/4)	100% (4/4)	100% (4/4)	1.00

N.A., not applicable. LD-DLIR, low-dose with deep learning image reconstruction.LD-IR, low-dose with adaptive statistical iteration reconstruction Veo; SD-IR, standard-dose with hybrid-iterative reconstruction technique.
Data are means ± 1 standard deviation.
[a]Value was significantly lower ($p < 0.017$) than those with SD-IR and LD-DLIR.
[b]Value was significantly greater ($p < 0.017$) than those with SD-IR.

LESION DETECTION

The radiologists, who were unaware of the number of lesions, independently evaluated the CT images for lesions including thyroid nodules, breast masses, lymphadenopathy, liver cysts, hepatic hemangiomas, liver metastases, pancreatic cysts, peritoneal dissemination, adrenal nodules, renal cysts, uterine masses, and ovarian masses. The reference standard for the presence of lesions was interpreted by the study coordinator (Y.N., with who had 9 years of post-training experience in interpreting body CT images). The study coordinator estimated the lesion size on PACS using electronic calipers.

QUANTITATIVE IMAGE ANALYSIS

Two radiologists independently and randomly measured the attenuation values (HU) of the liver, pancreas, spleen, abdominal aorta, and portal vein using a region of interest (ROI) of approximately 25–100 mm^2. ROI placement was performed in the right hepatic lobe parenchyma and body of pancreas while carefully avoiding blood vessels, bile ducts, pancreatic duct, focal lesions, and artifacts. ROI placement in the aorta was performed at the level of the first lumbar vertebral body avoiding of the vessel wall, calcifications, thrombi, and artifacts. For all measurements, the attenuation (in HU) was recorded along with the standard deviation (SD) for fat. The SD for fat was considered as an objective measure of image noise. The signal-to-noise ratio (SNR) of the liver, pancreas, and spleen was calculated by dividing the attenuation values of each anatomical structure by the background noise.

STATISTICAL ANALYSIS

Statistical analyses were performed using MedCalc Software for Windows (v.19.3.1). For qualitative analysis, the Friedman test was conducted to compare the confidence ratings for sharpness, image noise, and diagnostic acceptability of the SD-IR, LD-IR, and LD-DLIR images. The Fisher's exact-test was performed to compare the detectability of lesions of the SD-IR, LD-IR, and LD-DLIR images in a patient-by-patient analysis. For quantitative analysis, repeated-measure analysis of variance was conducted to evaluate differences between the SD-IR, LD-IR, and LD-DLIR images in terms of the attenuation values of the liver, pancreas, spleen, abdominal aorta, and portal vein, background noise, and SNR of the liver, pancreas, and spleen. When a significant difference was found between the three groups, pairwise comparisons were performed using the Wilcoxon or paired *t-test*s; and a stricter $p < 0.017$, introducing the Bonferroni correction, was considered statistically significant.

Inter-observer variability in qualitative and quantitative measurements was assessed using the κ statistic and the intraclass correlation coefficient (ICC), which measures the degree of

Figure 2. A 72-year-old male who underwent surgery for esophageal cancer. (a) Axial standard-dose portal venous phase image, (b) low-dose portal venous phase image reconstructed with ASiR-V of 40%, and (c) low-dose portal venous phase image reconstructed with TFI-H show enlarged mediastinal lymph node (arrow).

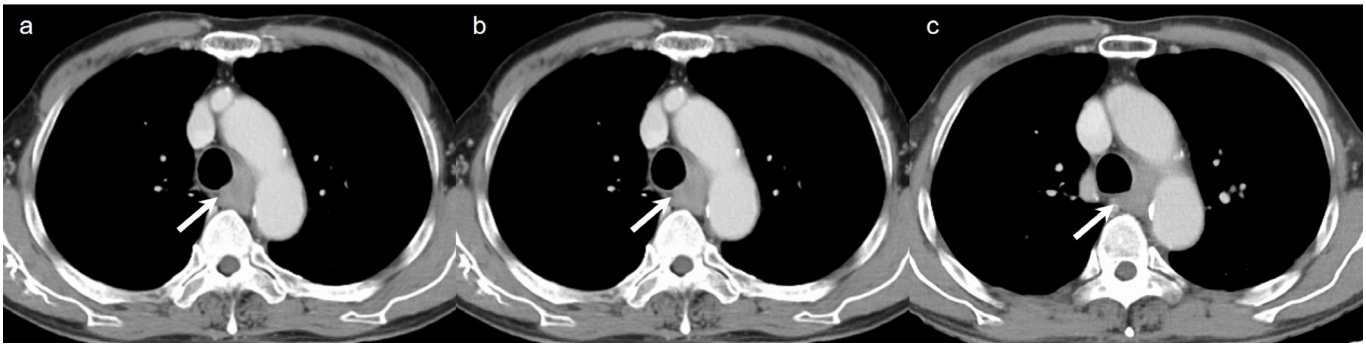

Figure 3. A 46-year-old male who underwent surgery for rectal cancer. (a) Axial standard-dose portal venous phase image, (b) low-dose portal venous phase image reconstructed with ASiR-V of 40%, and (c) low-dose portal venous phase image reconstructed with TFI-H show a tiny liver metastasis (arrow) and a liver cyst (arrowhead).

agreement between two radiologists. An ICC of <0.5 was interpreted as poor agreement, 0.50–0.75 as moderate agreement, 0.75–0.90 as good agreement, and ≥0.90 as excellent agreement.[21] A κ value of ≤0.20 was interpreted as slight agreement, 0.21–0.40 as fair agreement, 0.41–0.60 as moderate agreement, 0.61–0.80 as substantial agreement, and ≥0.81 as almost perfect agreement.

The Mann–Whitney *U* test was conducted to evaluate the differences in the $CTDI_{vol}$ and DLP between the SD and LD scans. *p*-values < 0.05 were considered statistically significant.

RESULTS

Patient demographics and lesion characteristics

Patient demographics and lesion characteristics are summarized in Table 2. The mean patient body weight and body mass index were 52.8 ± 10.7 kg and 20.8 ± 3.4, respectively. The following focal lesions were detected; 32 thyroid nodules in 22 patients, two breast masses in two patients, four lymphadenopathies in four patients, 107 liver cysts in 34 patients, nine hepatic hemangiomas in eight patients, 18 liver metastases in three patients, two pancreatic cysts in two patients, five counts of peritoneal dissemination in two patients, two adrenal nodules in two patients, 91 renal cysts in 37 patients, 11 uterine masses in seven patients, and five ovarian masses in four patients.

QUALITATIVE IMAGE ANALYSIS

Table 3 shows qualitative data for image quality and lesion detection, *p*-values, and κ values. All *p*-values are the results of the Friedman and Fisher's exact tests. Significant difference in the pairwise comparisons are shown using marks in the Table and the descriptions below the Table.

IMAGE QUALITY

The sharpness, image noise, and diagnostic acceptability were significantly worse in the LD-IR than in the SD-IR and LD-DLIR ($p < 0.017$), however, there was no significant difference in terms of the sharpness and diagnostic acceptability between the SD-IR and LD-DLIR. Image noise was significantly more improved in the LD-DLIR than in the SD-IR ($p < 0.017$). The κ values ranged from 0.24 to 0.68, indicating fair to substantial agreement between the two readers.

LESION DETECTION

All patients with breast masses ($n = 2$), lymphadenopathy ($n = 4$), liver metastases ($n = 3$), pancreatic cysts ($n = 2$), peritoneal dissemination ($n = 2$), adrenal nodules ($n = 2$), and ovarian masses ($n = 4$) were detected on the SD-IR, LD-IR, and LD-DLIR images both in readers 1 and 2. Patients with the following focal lesions were missed on all of the SD-IR, LD-IR, and LD-DLIR: three liver cysts in reader 2, one hepatic hemangioma in reader 2, one uterine mass both in readers 1 and 2. Two patients with thyroid nodules were missed on the SD-IR, and an additional one was missed on the LD-IR and LD-DLIR in reader 2. One patient with a liver cyst was missed both on the LD-IR and LD-DLIR in reader 1. Two patients with renal cysts were missed on the SD-IR and LD-DLIR, and an additional two were missed on the LD-IR in reader 1. One patient with renal cysts was missed both on the LD-IR and LD-DLIR in reader 2. The lesion sizes which were missed on LD CT was 3.5 mm for the thyroid nodule, 3.5 mm for the liver cyst, 2.4 mm and 4.6 mm for the renal cysts. However, there was no significant difference in the sensitivity for detecting each lesion between the CT images ($p = 0.73–1.00$) (Figures 2 and 3). Additionally, no false-positive lesion was found in this study.

QUANTITATIVE IMAGE ANALYSIS

Table 4 shows quantitative data, *p*-values, and ICCs. All *p*-values are the results of the repeated-measure analysis of variance. Significant difference in the pairwise comparisons are shown using marks in the Table and the descriptions below the Table.

No significant difference was found in attenuation values of the liver, pancreas, spleen, abdominal aorta, and portal vein between the various CT images ($p = 0.28–0.96$). The background noise was significantly higher in the LD-IR than in the SD-IR and LD-DLIR, and was significantly lower in the LD-DLIR than in the SD-IR ($p < 0.001$). Except for the SNR of the spleen in reader 2, the SNRs were significantly lower in the LD-IR than in the SD-IR and LD-DLIR, and were significantly higher in the LD-DLIR than in the SD-IR ($p < 0.001$). The ICCs ranged from 0.28 to 0.98, indicating poor to excellent agreement between the two readers.

Table 4. Attenuation Values and Signal-to-Noise Ratio

	SD-IR	LD-IR	LD-DLIR	*p*-value
Attenuation value				
Liver (ICC)	0.85	0.92	0.94	N.A.
Reader 1	120.9 ± 11.6 (97.7–149.1)	119.3 ± 9.9 (74.8–136.4)	119.6 ± 9.8 (75.8–137.1)	0.66
Reader 2	120.9 ± 12.7 (95.5–158.4)	120.3 ± 10.7 (74.3–142.3)	120.4 ± 10.5 (73.9–140.6)	0.96
Pancreas (ICC)	0.71	0.87	0.85	N.A.
Reader 1	104.2 ± 11.3 (78.9–129.7)	105.6 ± 12.2 (80.3–131.8)	106.0 ± 12.3 (79.3–134.8)	0.72
Reader 2	102.5 ± 14.3 (64.7–134.2)	102.3 ± 14.0 (67.2–127.3)	103.5 ± 13.2 (70.6–128.8)	0.88
Spleen (ICC)	0.90	0.89	0.66	N.A.
Reader 1	133.5 ± 14.2 (101.5–162.6)	130.7 ± 11.1 (109.1–160.0)	130.0 ± 10.8 (103.1–156.0)	0.28
Reader 2	134.0 ± 12.3 (109.1–163.5)	131.0 ± 10.6 (111.9–162.4)	131.3 ± 10.6 (113.4–162.8)	0.32
Abdominal aorta (ICC)	0.91	0.96	0.98	N.A.
Reader 1	161.1 ± 19.3 (122.5–198.8)	159.8 ± 17.1 (115.0–202.5)	161.5 ± 17.5 (114.9–206.1)	0.87
Reader 2	163.4 ± 21.4 (123.8–214.6)	160.8 ± 18.4 (112.6–206.8)	161.9 ± 18.3 (112.9–207.8)	0.76
Portal vein (ICC)	0.87	0.90	0.94	N.A.
Reader 1	175.8 ± 19.4 (136.2–212.3)	175.6 ± 16.8 (141.6–220.2)	178.7 ± 17.2 (142.5–224.2)	0.57
Reader 2	178.8 ± 23.3 (122.4–244.4)	173.9 ± 18.0 (137.3–214.7)	177.7 ± 18.4 (137.6–218.4)	0.39
Background noise (ICC)	0.41	0.28	0.31	N.A.
Reader 1	7.5 ± 1.7 (4.2–12.9)	11.0 ± 1.7[a] (6.7–15.4)	6.5 ± 1.8[b] (4.1–13.7)	<0.001
Reader 2	8.3 ± 1.9 (5.1–12.6)	11.7 ± 1.4[a] (8.4–15.2)	7.5 ± 2.1[b] (4.5–14.6)	<0.001
SNR				
Liver (ICC)	0.55	0.35	0.39	N.A
Reader 1	16.9 ± 3.7 (9.9–26.5)	11.1 ± 1.8[c] (7.9–17.7)	19.5 ± 4.0[d] (9.4–29.3)	<0.001
Reader 2	15.6 ± 4.5 (8.4–26.7)	10.5 ± 1.4[c] (6.9–13.9)	17.3 ± 4.5[d] (8.3–26.5)	<0.001
Pancreas (ICC)	0.47	0.31	0.52	N.A.
Reader 1	14.5 ± 3.4 (7.6–27.3)	9.8 ± 1.7[c] (6.3–15.5)	17.1 ± 3.7[d] (6.9–23.7)	<0.001
Reader 2	13.2 ± 3.5 (7.7–23.7)	8.9 ± 1.4[c] (5.3–11.7)	14.8 ± 4.0[d] (7.1–22.0)	<0.001
Spleen (ICC)	0.55	0.42	0.50	N.A.
Reader 1	18.9 ± 4.7 (9.7–38.4)	12.2 ± 1.9[c] (8.0–17.6)	21.4 ± 5.0[d] (8.8–35.1)	<0.001
Reader 2	17.3 ± 5.1 (8.7–29.1)	11.4 ± 1.7[c] (7.7–17.0)	18.9 ± 5.2 (8.0–29.2)	<0.001

N.A., not applicable. ICC, intraclass correlation coefficient.LD-DLIR, low-dose with deep learning image reconstruction; LD-IR, low-dose with adaptive statistical iteration reconstruction Veo.SD-IR, standard-dose with hybrid-iterative reconstruction technique.SNR, signal-to-noise ratio..
Data are means ± 1 standard deviation.
[a]Value was significantly greater ($p < 0.017$) than those with SD-IR and LD-DLIR.
[b]Value was significantly lower ($p < 0.017$) than those with SD-IR.
[c]Value was significantly lower ($p < 0.017$) than those with SD-IR and LD-DLIR.
[d]Value was significantly greater ($p < 0.017$) than those with SD-IR.

RADIATION DOSE

The mean $CTDI_{vol}$ (2.9 ± 0.8 mGy; range, 1.4–4.8 mGy) and DLP (216.2 ± 65.8 mGy•cm; range, 95.2–396.0 mGy•cm) were significantly lower in the LD CT scan than those in SD scan (mean $CTDI_{vol}$, 13.5 ± 4.1 mGy; range, 6.7–23.6 mGy and mean DLP, 1011.6 ± 340.2 mGy•cm; range, 469.3–1955.8 mGy•cm) ($p < 0.0001$) (Table 5). The average reduction rates of the mean $CTDI_{vol}$ and DLP were 78.5% and 78.6%, respectively.

DISCUSSION

Our study demonstrated that LD CT reconstructed with DLIR allows >75% radiation dose reduction while maintaining image quality and lesion detectability in comparison to SD-IR, while providing better image quality than LD-IR. LD CT reconstructed with hybrid- or full-IR has been shown to allow significant radiation dose reduction in routine clinical practice.[11,12] We recruited patients with malignant tumor in this study in order to test the

Table 5. Radiation Dose in Standard- and Low-dose CT protocols

	Standard-dose	Low-dose	*p*-value
CTDIvol (mGy)	13.5 ± 4.1 (6.7–23.6)	2.9 ± 0.8 (1.4–4.8)	<0.0001
DLP (mGy*cm)	1011.6 ± 340.2 (469.3–1955.8)	216.2 ± 65.8 (95.2–396.0)	<0.0001

$CTDI_{vol}$, CT dose index volume;.DLP, dose-length product.
Data are means ± 1 standard deviation.

utility of DLIR for radiation dose reduction and lesion detection. The findings of this study are, however, most applicable in patients with chronic disease processes or young patients with low grade tumors.

LD CT reconstructed with full-IR had significantly worse contrast resolution and diagnostic acceptability in comparison to hybrid-IR.[12] LD CT reconstructed with DLIR images have been shown to be preferred by radiologists in contrast to hybrid- and full-IR.[15] In comparison with SD CT, the image quality was comparable between SD CT reconstructed with hybrid-IR and LD CT reconstructed with DLIR.[17] DLIR is a very promising image reconstruction algorithm which facilitates reduction in radiation dose while maintaining diagnostic image quality and is preferred by radiologists.

We found that lesion detection was not significantly different between the SD-IR, LD-IR, and LD-DLIR images. A few lesions were missed on the LD-IR and LD-DLIR images, but there was no significant difference in the sensitivity among the CT images (p = 0.73–1.00). Singh R et al[17] reported that some clinically significant lesions are missed on LD with hybrid-IR images, but all of these lesions are detected on LD with DLIR images. We believe the reason why the LD-DLIR could be of comparable lesion detection to the SD-IR was good image quality and less image noise.

Although there was no significant difference in CT numbers of anatomical structures among the SD-IR, LD-IR, and LD-DLIR, the background noise was significantly reduced in the LD-DLIR compared to the SD-IR and LD-IR images. As a result, the SNRs of the liver, pancreas, and spleen were significantly greater in the LD-DLIR than those in the SD-IR and LD-IR. In our study, the mean body weight and body mass index of patients were 52.8 kg (range, 33.0–82.0 kg) and 20.8 (range, 13.0–29.5), respectively, which might be smaller body weight and body mass index distribution than that of a Western population. Although we need a further clinical study with large-body-size patients to validate our results, we guess this LD protocol might be applied to large-body-size patients. Since majority of oncological patients can have reduced body weight, the findings of our study are applicable to the oncological population, and additionally, in patients with inflammatory bowel disease as well. However, although when our LD protocol will be applied to large-body-size patients, the background noise will increase and the SNR will decrease, the background noise is still lower and the SNR is still greater in the LD-DLIR compared to the SD-IR images at this moment.

There were several limitations to this study. First, the study population was relatively small and our investigation was carried out at a single institution. Second, we only evaluated lesion detection among the SD-IR, LD-IR, and LD-DLIR using a patient-by-patient analysis. Third, as described above, the body size of patients was small. Finally, we only used a CT scanner from a single vendor. Therefore, further clinical studies of larger populations are required to validate our results for other brands of CT scanners.

In conclusion, DLIR allows substantial radiation dose reduction of >75% with significant improvements in the background noise and SNR enabling confident diagnosis and acceptable image quality.

CONFLICT OF INTEREST

AK: Grant support for research activities from Philips and GE Healthcare. Other authors report no relevant disclosures or conflicts of interest.

REFERENCES

1. Guglielmo FF, Anupindi SA, Fletcher JG, Al-Hawary MM, Dillman JR, Grand DJ, et al. Small bowel Crohn disease at CT and Mr Enterography: imaging atlas and glossary of terms. *Radiographics* 2020; **40**: 354–75. doi: https://doi.org/10.1148/rg.2020190091
2. Kambadakone AR, Eisner BH, Catalano OA, Sahani DV. New and evolving concepts in the imaging and management of urolithiasis: urologists' perspective. *Radiographics* 2010; **30**: 603–23. doi: https://doi.org/10.1148/rg.303095146
3. Pickhardt PJ, Graffy PM, Said A, Jones D, Welsh B, Zea R, et al. Multiparametric CT for noninvasive staging of hepatitis C virus-related liver fibrosis: correlation with the histopathologic fibrosis score. *AJR Am J Roentgenol* 2019; **212**: 547–53. doi: https://doi.org/10.2214/AJR.18.20284
4. Wulff AM, Bolte H, Fischer S, Freitag-Wolf S, Soza G, Tietjen C, et al. Lung, liver and lymph node metastases in follow-up MSCT: comprehensive volumetric assessment of lesion size changes. *Rofo* 2012; **184**: 820–8. doi: https://doi.org/10.1055/s-0032-1312860
5. Tezcan D, Türkvatan A, Türkoğlu MA, Bostancı EB, Sakaoğullları Z. Preoperative staging of colorectal cancer: accuracy of single portal venous phase multidetector computed tomography. *Clin Imaging* 2013; **37**: 1048–53. doi: https://doi.org/10.1016/j.clinimag.2013.08.003

6. Baskan O, Erol C, Ozbek H, Paksoy Y. Effect of radiation dose reduction on image quality in adult head CT with noise-suppressing reconstruction system with a 256 slice MDCT. *J Appl Clin Med Phys* 2015; **16**: 285–96. doi: https://doi.org/10.1120/jacmp.v16i3.5360
7. Hara AK, Paden RG, Silva AC, Kujak JL, Lawder HJ, Pavlicek W. Iterative reconstruction technique for reducing body radiation dose at CT: feasibility study. *AJR Am J Roentgenol* 2009; **193**: 764–71. doi: https://doi.org/10.2214/AJR.09.2397
8. Silva AC, Lawder HJ, Hara A, Kujak J, Pavlicek W. Innovations in CT dose reduction strategy: application of the adaptive statistical iterative reconstruction algorithm. *AJR Am J Roentgenol* 2010; **194**: 191–9. doi: https://doi.org/10.2214/AJR.09.2953
9. Marin D, Nelson RC, Schindera ST, Richard S, Youngblood RS, Yoshizumi TT, et al. Low-tube-voltage, high-tube-current multidetector abdominal CT: improved image quality and decreased radiation dose with adaptive statistical iterative reconstruction algorithm--initial clinical experience. *Radiology* 2010; **254**: 145–53. doi: https://doi.org/10.1148/radiol.09090094
10. Noda Y, Goshima S, Koyasu H, Shigeyama S, Miyoshi T, Kawada H, et al. Renovascular CT: comparison between adaptive statistical iterative reconstruction and model-based iterative reconstruction. *Clin Radiol* 2017; **72**: 901.e13–901.e19. doi: https://doi.org/10.1016/j.crad.2017.06.002
11. Han WK, Na JC, Park SY. Low-Dose CT angiography using ASiR-V for potential living renal donors: a prospective analysis of image quality and diagnostic accuracy. *Eur Radiol* 2020; **30**: 798–805. doi: https://doi.org/10.1007/s00330-019-06423-1
12. Moloney F, James K, Twomey M, Ryan D, Grey TM, Downes A, et al. Low-Dose CT imaging of the acute abdomen using model-based iterative reconstruction: a prospective study. *Emerg Radiol* 2019; **26**: 169–77. doi: https://doi.org/10.1007/s10140-018-1658-z
13. Xin X, Shen J, Yang S, Liu S, Hu A, Zhu B, et al. Improved image quality of low-dose CT combining with iterative model reconstruction algorithm for response assessment in patients after treatment of malignant tumor. *Quant Imaging Med Surg* 2018; **8**: 648–57. doi: https://doi.org/10.21037/qims.2018.08.05
14. McCollough CH, Yu L, Kofler JM, Leng S, Zhang Y, Li Z, et al. Degradation of CT low-contrast spatial resolution due to the use of iterative reconstruction and reduced dose levels. *Radiology* 2015; **276**: 499–506. doi: https://doi.org/10.1148/radiol.15142047
15. Padole A, Ali Khawaja RD, Kalra MK, Singh S. Ct radiation dose and iterative reconstruction techniques. *AJR Am J Roentgenol* 2015; **204**: W384–92. doi: https://doi.org/10.2214/AJR.14.13241
16. Akagi M, Nakamura Y, Higaki T, Narita K, Honda Y, Zhou J, et al. Deep learning reconstruction improves image quality of abdominal ultra-high-resolution CT. *Eur Radiol* 2019; **29**: 6163–71. doi: https://doi.org/10.1007/s00330-019-06170-3
17. Singh R, Digumarthy SR, Muse VV, Kambadakone AR, Blake MA, Tabari A, et al. Image quality and lesion detection on deep learning reconstruction and iterative reconstruction of Submillisievert chest and abdominal CT. *AJR Am J Roentgenol* 2020; **214**: 566–73. doi: https://doi.org/10.2214/AJR.19.21809
18. Rengo M, Bellini D, De Cecco CN, Osimani M, Vecchietti F, Caruso D, et al. The optimal contrast media policy in CT of the liver. Part I: technical notes. *Acta Radiol* 2011; **52**: 467–72. doi: https://doi.org/10.1258/ar.2011.100499
19. JHsieh JLE, Nett B, Tang J, Thibault JB, Sahney S. A new era of image reconstruction: TrueFidelity™. technical white paper on deep learning image reconstruction. *GE Healthcare* 2019;.
20. Greffier J, Hamard A, Pereira F, Barrau C, Pasquier H, Beregi JP, et al. Image quality and dose reduction opportunity of deep learning image reconstruction algorithm for CT: a phantom study. *Eur Radiol* 2020; **30**: 3951–9. doi: https://doi.org/10.1007/s00330-020-06724-w
21. Koo TK, Li MY, . A guideline of selecting and reporting intraclass correlation coefficients for reliability research. *J Chiropr Med* 2016; **15**: 155–63. doi: https://doi.org/10.1016/j.jcm.2016.02.012